frontiers in Earth Science

ORIGINAL RESEARCH
published: 31 March 2022
doi: 10.3389/feart.2022.861847

Fractal Characteristics and Energy Dissipation of Granite After High-Temperature Treatment Based on SHPB Experiment

Lei Liu[1,2], *Yuan Wang*[1] *and Huaming An*[3]*

[1]Faculty of Land Resources Engineering, Kunming University of Science and Technology, Kunming, China, [2]Key Laboratory for Development and Utilization of Sino German Blue Mine and Special Underground Space in Yunnan Province, Kunming University of Science and Technology, Kunming, China, [3]Faculty of Public Security and Emergency Management, Kunming University of Science and Technology, Kunming, China

In deep mining and high-concentration nuclear waste storage engineering, the surrounding rocks may be subjected to the combined action of high-temperature fire and impact load. In this study, the fracture morphology and the energy dissipation of granite following high-temperature treatment at 25–800°C were analyzed using the split Hopkinson pressure bar (SHPB) device. The fracture characteristics and the dynamic mechanical properties of granite were determined. The energy dissipation of granite specimens affected by high temperatures in the SHPB experiment was also analyzed. When the temperature of the impact rate was less than 200°C, the fragmentation degree, transmitted energy, and dissipated energy of granite increased with an increase in temperature. When the temperature was higher than 200°C, the change law was opposite. A strong linear correlation existed among the fragmentation, fractal dimension, and energy consumption density of granite at different impact rates after high-temperature treatment. Moreover, a strong quadratic correlation existed between the damage factors and temperature. When the temperature was less than 200°C, the damage factor decreased with the increase in temperature. When the temperature was higher than 200°C, the change law was opposite, which corresponded with the influence law of temperature on dynamic compressive strength. Scanning electron microscopy and X-ray diffraction analyses were conducted to study the fracture modes and mineral composition changes in the granites. A quantitative relationship existed between macro- and meso-properties. The results could provide theoretical basis for the design of underground engineering structures, post-disaster assessment, and rehabilitation activities.

Keywords: high temperature, granite, energy dissipation, fractal dimension, SHPB

OPEN ACCESS

Edited by:
Zhiqiang Yin,
Anhui University of Science and Technology, China

Reviewed by:
Zhaozhao Chang,
Zhejiang University of Technology, China
Chongchong Qi,
Central South University, China
Yang Liu,
Anhui Jianzhu University, China

***Correspondence:**
Huaming An
huaming.an@kust.edu.cn

Specialty section:
This article was submitted to Geohazards and Georisks, a section of the journal Frontiers in Earth Science

Received: *25 January 2022*
Accepted: *28 February 2022*
Published: *31 March 2022*

Citation:
Liu L, Wang Y and An H (2022) Fractal Characteristics and Energy Dissipation of Granite After High-Temperature Treatment Based on SHPB Experiment. Front. Earth Sci. 10:861847. doi: 10.3389/feart.2022.861847

INTRODUCTION

During deep mining and deep underground engineering constructions, deep surrounding rocks inevitably encounter "three high and one disturbance" environments (Xie, 2019). Moreover, drilling and blasting, large-scale mechanical vibration, and other engineering activities produce dynamic impact loads. High temperatures and dynamic disturbances affect the stability of deep surrounding rocks (Sasmito et al., 2015; Yuan et al., 2011), thereby posing huge threat to the safety of deep resource exploration and deep underground engineering construction personnel (Qi et al., 2021). By

studying the internal energy variation characteristics of the rock material affected by high temperature under impact load, the dynamic mechanical properties of rock materials affected by high temperature can be comprehensively analyzed. This provides a theoretical basis for the structural design and safety evaluation of the surrounding rock during deep resource exploration and deep underground engineering construction (Li et al., 2021).

In terms of statics, the change rule of rock properties after high-temperature treatment was studied using conventional uniaxial compression tests and non-destructive monitoring (Bandini and Berry, 2012; Brotóns et al., 2013; Liu and Xu, 2015; Wang et al., 2013). With the increase in temperature, the strength, elastic modulus, and p-wave velocity of the rock all exhibited a decreasing trend. In engineering practice, the stability of the surrounding rock is typically associated with the dynamic impact load. With the development and application of split Hopkinson pressure bar (SHPB) technology, researchers have conducted relevant studies on the mechanical properties of rocks at normal and high temperatures (Yin et al., 2016b; Imani et al., 2017; Malik et al., 2018; Yin et al., 2019). Mishra et al. (2018) studied the dynamic mechanical responses of three types of magmatic rocks using a small-diameter SHPB device. They revealed that the strain rate effect was evident and proposed a correlation equation for the granite dynamic growth factor. Liu and Xu (2014) studied the mechanical properties of granite at high temperatures using an SHPB test system and found that there is a critical temperature that causes structural changes and mechanical deterioration in the granite. Through dynamic compression experiments, Yin et al. (2011) found that temperature promoted the evaporation of water inside the rock, decomposition of mineral particles, and reduction of internal bonding force, resulting in sandstone fragments tending to be fine-grained after dynamic impact with an increase in temperature. Rock damage always accompanies energy conversion and consumption. The dynamic impact failure of rocks is a process of energy input, absorption, and release (Xu and Shi, 2013). Yin et al. (2016a) studied the energy consumption law of the dynamic impact compression tests of coal and rock under high temperatures. They found that the reflected energy increased with increasing temperature, whereas the transmitted energy and absorbed energy exhibited opposite trends. Zhang and Jing (2018) analyzed the energy dissipation of sandstone after dynamic impact under high and low temperatures and found that the change in incident energy and absorbed energy was divided at −5 and 400°C. It increased with increasing temperature before the cutoff point and, thereafter, decreased with increasing temperature. Some researchers have linked the dissipated energy to the degree of breakage. They found that the specific energy absorption increased linearly with the incident energy and exhibited an exponential relationship with average fragmentation (Hong et al., 2009). Wu et al. (2019, 2020) analyzed the dynamic failure modes and the impact fragmentation of phyllites with different bedding angles considering the incident energy, energy absorption, and wave propagation characteristics. Ji et al. (2020) explored the fractal characteristics of the dynamic impact breakage of granite and sandstone using an SHPB test system. They found that the fractal dimension could quantitatively analyze crushing energy consumption and fragmentation.

In recent years, comparative studies on the energy absorption value, fractal dimension, and fracture morphology have been sufficient. However, there are few reports on the energy evolution law of rock materials affected by temperature during dynamic impact compression and considering the fractal dimension from the perspective of fracture conditions. The formation of granite iron, copper, gold, and tin ores is closely related (He, 1994). Therefore, granite was selected as the research object in this study. Dynamic impact compression tests were conducted on granite specimens treated at room temperature (25°C) and high temperatures (200°C, 400 °C, 600°C, and 800°C). A standard circular hole screen was used to screen and count the granite broken test blocks after the dynamic impact compression. The variations in the peak stress, fracture morphology, and energy dissipation of granite specimens with temperature grade were studied.

EXPERIMENTS

Preparation and High-Temperature Treatment of Granite Samples

Granite samples were obtained from the Kafang tin mine in Honghe Hani and Yi Autonomous Prefecture, Yunnan Province, China. According to the International Society for Rock Mechanics (ISRM) standard (Zhou et al., 2012), granite was processed into a cylindrical sample with a diameter of 50 mm and an aspect ratio of 0.5. A KRX-17B box-type resistance furnace was used to treat granite samples at high temperatures. The heating rate was set at 2°C/min. After heating to the target temperature, the temperature was maintained constant for 2 h. After heating, the sample was cooled to room temperature (25°C) in a furnace chamber before removal. To prevent the reaction between the rock samples and water vapor in the air following the high-temperature treatment, the samples were stored in a Tester WGLL-230BE electric blast-drying oven. The granite specimen after high-temperature treatment is shown in **Figure 1**. Evidently, with an increase in the heating temperature, the surface color of the granite specimens gradually deepened. When the heating temperature exceeded 400°C, thermal cracks appeared on the surface of granite specimens.

SHPB Testing System

Figure 2 shows the schematic of a 50 mm diameter SHPB test system used in this study. The system includes a dynamic loading part (nitrogen tank, gas gun, and spindle punch), rod part (incident bar and transmission bar), and data acquisition part (infrared speed measuring, single recording device, and data-processing device). The incident, transmission, and impact bars were all ^{40}Cr high-strength alloy steels. The density was 7.81 g/cm^3. The lengths of the incident rod and transmission rod were 2 m. The longitudinal wave velocity was 5,100 m/s. The elastic modulus was 210 GPa. The strain gauge was pasted on 1/2 of the rod.

During the SHPB experiment, the sample was placed between the incident and transmission bars, and the bullet was discharged at a certain speed. A stress wave was thus formed in the incident

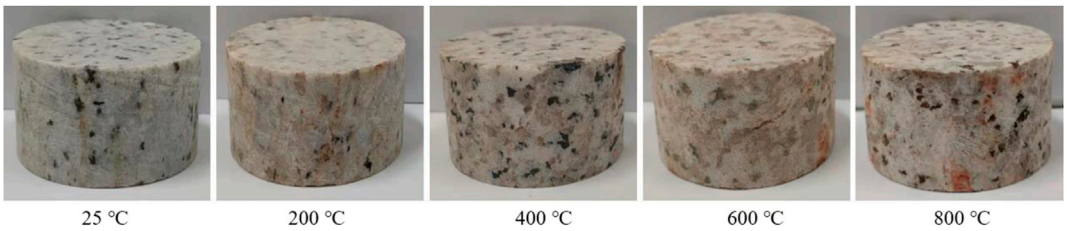

FIGURE 1 | Granite specimen after high-temperature treatment.

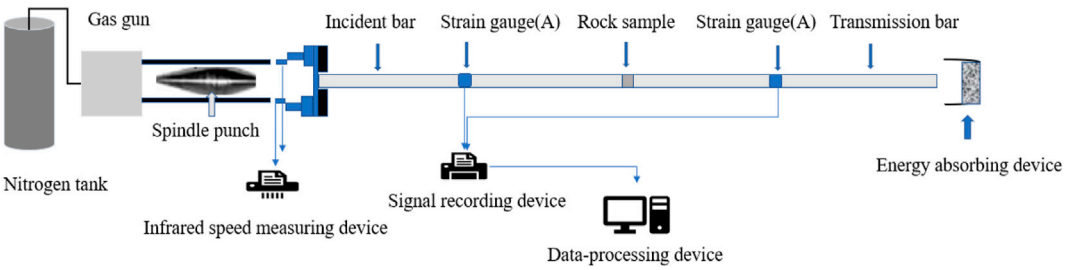

FIGURE 2 | Schematic of the split Hopkinson pressure bar device.

bar after impacting the incident bar. The incident waves were then propagated forward in the incident bar. When transmitted to the interface between the incident rod and the sample, a part of the incident wave was reflected back to the incident rod as a reflected wave, owing to the wave impedance difference between the rod and the sample. The other part was transmitted through the sample into the transmission rod as a transmission wave. Based on the one-dimensional stress assumption and stress uniformity assumption (Hu et al., 2015), the following method was described by Wang (2005). By substituting the signal collected by the strain gauge in **Eq. 1**, the stress $\sigma(t)$, strain $\varepsilon(t)$, and strain rate $\dot{\varepsilon}(t)$ of the specimen can be obtained as follows:

$$\left.\begin{aligned}\sigma(t) &= \frac{EA}{2A_s}\left[\varepsilon_i(t)+\varepsilon_r(t)+\varepsilon_t(t)\right]\\ \dot{\varepsilon}(t) &= \frac{C}{l_s}\left[\varepsilon_i(t)-\varepsilon_r(t)-\varepsilon_t(t)\right]\\ \varepsilon(t) &= \frac{C}{l_s}\int_0^t\left[\varepsilon_i(t)-\varepsilon_r(t)-\varepsilon_t(t)\right]dt\end{aligned}\right\}, \quad (1)$$

where $\varepsilon_i(t)$, $\varepsilon_r(t)$, and $\varepsilon_t(t)$ are the incident, reflected, and transmitted strains on the bar, respectively; A, E, and C represent the cross-sectional area, elastic modulus, and longitudinal wave velocity of the pressure rod, respectively.

Experimental Scheme

In this experiment, the granite specimens were heated and naturally cooled at room temperature (25°C) and high temperatures at different temperature levels (200°C, 400°C, 600°C, and 800°C). The specimens were then subjected to the dynamic impact compression experiments at different impact velocities (8.5 m/s, 11.5 m/s, and 13.5 m/s). The standard circular hole screens with different diameters (0.3, 0.5, 1, 2.5, 5, 10, 15, 20, and 25 mm) were used to screen the granite fragments following the experiment. A total of three-independent experiments were conducted for each working condition. Statistically significant data were selected for statistical analysis.

To ensure the validity of the experimental data, the stress balance must be ensured at both ends of the rock sample before the dynamic impact compression test. Typical waveforms at both ends of the sample are shown in **Figure 3A**. **Figure 3B** shows that the overlapping waveforms of the incident and reflection stresses have a high degree of coincidence with those of the transmission stress, which can guarantee the stress balance state in the dynamic impact process and the validity of the test data results.

SHPB Dynamic Stress–Strain Curve

The dynamic stress–strain curves of the granite specimens affected by different temperatures at different impact rates are shown in **Figure 4**.

As shown in **Figure 4**, the dynamic stress–strain curves of granite can be roughly divided into three stages: elasticity, yield, and failure. The initial stage of the curve was approximately a straight line, indicating that granite had a strong linear elastic relationship during the initial stage of dynamic impact compression. The slope of the curve at this stage can be approximated as the initial elastic modulus of rock. The stress–strain curve at the same impact rate initially moved up slightly and then moved sharply to the lower right along with the position of the ascending curve of the temperature grade. The initial elastic modulus and peak stress of the rock first increased

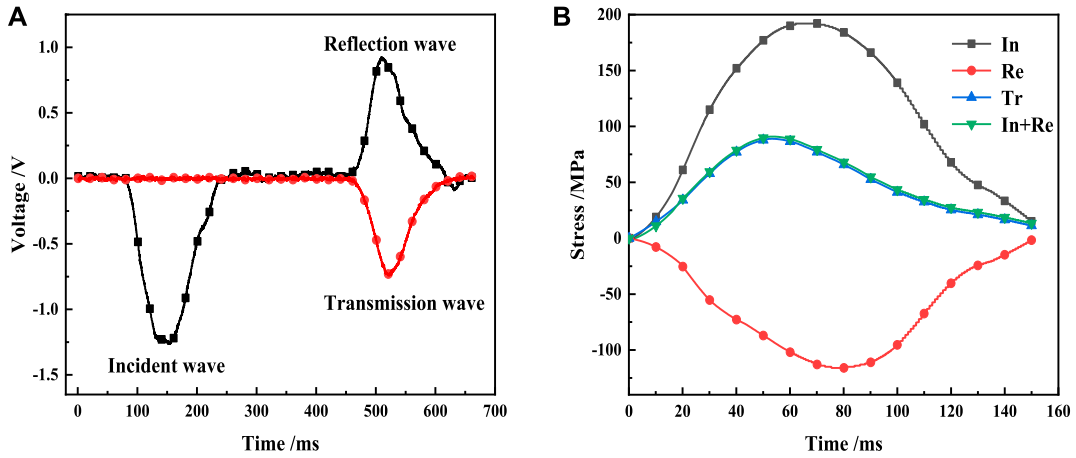

FIGURE 3 | Typical waveforms at both ends of the sample.

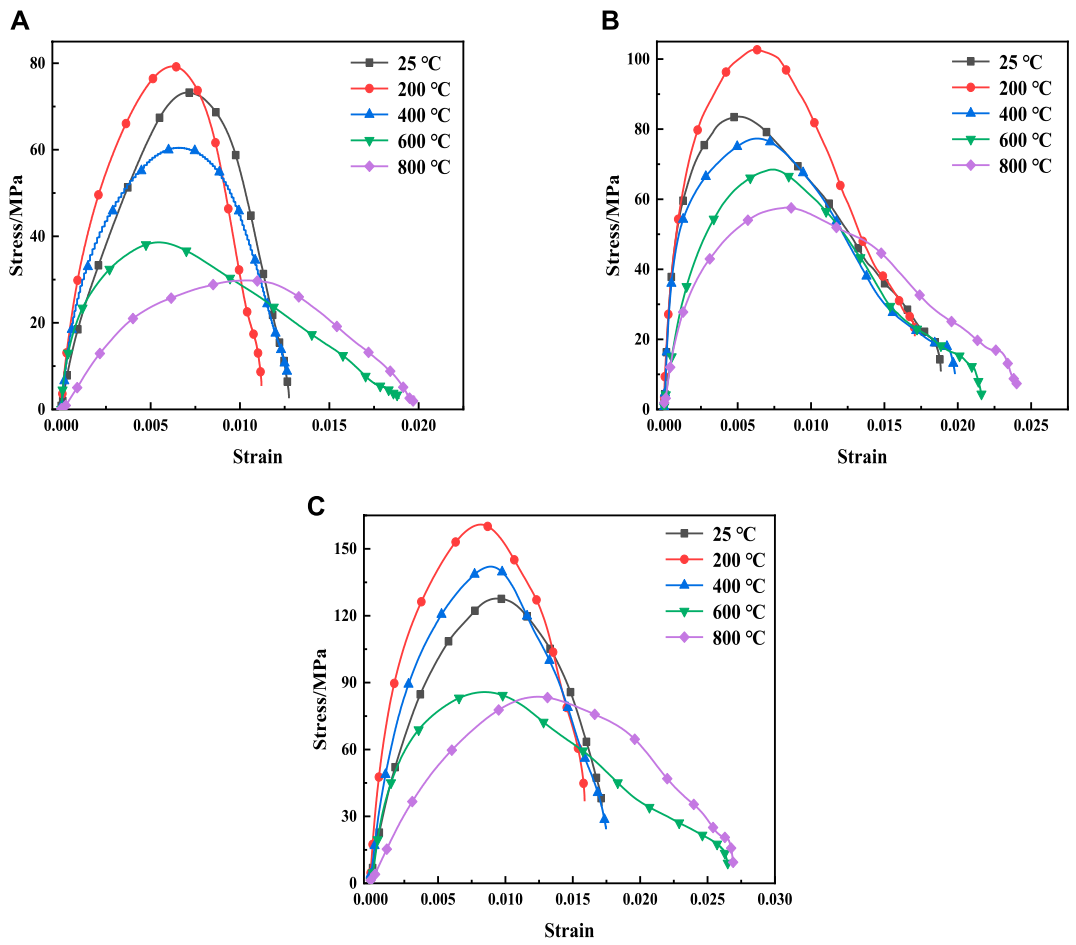

FIGURE 4 | Dynamic stress–strain curves of granite specimens affected by different temperatures at different impact velocities of **(A)** 8.5 m/s, **(B)** 11.5 m/s, and **(C)** 13.5 m/s.

TABLE 1 | Energy dissipation of granite under different working conditions.

Temperature (°C)	Impact velocity (m/s)	Incident energy W_I/J	Reflected energy W_R/J	Transmission energy W_T/J	Dissipation energy W_S/J	SEA J/cm^3
25	8.5	54.57	19.15	12.73	22.69	0.462
	11.5	108.94	41.72	19.36	47.86	0.976
	13.5	154.69	55.52	30.07	69.10	1.408
200	8.5	55.75	14.65	16.35	24.75	0.504
	11.5	114.71	36.91	25.95	51.85	1.057
	13.5	150.54	40.37	36.80	73.37	1.496
400	8.5	53.22	18.10	12.45	22.67	0.462
	11.5	111.88	48.25	18.49	45.14	0.920
	13.5	162.27	60.10	39.14	63.03	1.285
600	8.5	53.94	25.11	8.24	20.59	0.420
	11.5	113.65	59.27	11.26	43.12	0.879
	13.5	161.46	77.91	31.75	51.80	1.056
800	8.5	54.42	31.99	3.86	18.57	0.379
	11.5	112.27	67.58	8.03	36.66	0.747
	13.5	157.35	89.58	25.29	42.48	0.866

and then decreased. They reached the maximum at 200°C. The curve moved down significantly at 400°C than at normal temperature and 200°C, indicating that there is a threshold temperature for the deterioration of rock mechanical properties between 200 and 400°C. At 25–800°C, the curve gradually moved to the lower right. Thus, the continuous increase in rock failure strain indicates that the ductility of the rock was enhanced by high temperature, and it transitioned from brittleness to plasticity. With an increase in the strain rate at the same temperature level, the peak stress and elastic modulus of the rock have different degrees of buoyancy, which is an evident strain rate effect.

RESULTS AND DISCUSSION

Energy Dissipation

The development of fractures in rocks is the result of energy absorption (Xia et al., 2006; Zhao et al., 2019). **Eq. 2** was used to calculate the incident, reflected, transmitted, and dissipated energies during the dynamic impact compression tests of granite, as presented in **Table 1**.

$$\left.\begin{aligned} W_I &= ACE\int_0^t \varepsilon_i^2(t)d(t) \\ W_R &= ACE\int_0^t \varepsilon_r^2(t)d(t) \\ W_T &= ACE\int_0^t \varepsilon_t^2(t)d(t) \end{aligned}\right\}, \tag{2}$$

where W_I represents the incident energy; W_R represents the reflected energy; and W_T represents the transmitted energy; $\varepsilon_i(t)$, $\varepsilon_r(t)$, and $\varepsilon_t(t)$ are the incident, reflected, and transmitted strains on the bar, respectively; and A, E, and C represent the cross-sectional area, elastic modulus, and longitudinal wave velocity of the pressure rod, respectively.

The relationship among the incident, reflected, and transmitted energies under different working conditions is shown in **Figure 5**. At the same temperature, the energy levels of the incident, reflected, and transmitted energies increased with an increase in the impact rate. The growth rate was also positively correlated with the impact rate, exhibiting an evident strain rate effect. This conforms to the relevant laws of kinetic energy theorem (Shu et al., 2019). The influence of temperature was primarily reflected in the evolution of reflected and transmitted energies. With an increase in temperature, the transmission energy first increased and reached a maximum value at 200°C. When the temperature level exceeded 400°C, the transmitted energy gradually decreased with an increase in temperature; however, the effect on reflected energy was the opposite.

The influence of reflected or transmitted energy on granite specimens cannot be directly characterized by the influence of temperature on granite specimens during the crushing process. Xia et al. (2006) introduced the concept of crushing energy (**Eq. 3**) to characterize the energy dissipation during granite destruction.

$$W_S = W_I - [W_R + W_T], \tag{3}$$

where W_S represents the dissipated energy, W_I represents the incident energy, W_R represents the reflected energy, and W_T represents the transmitted energy.

Compared with other dissipated energies (such as heat energy), previous studies (Zhang and Jing, 2018; Shu et al., 2019) have considered dissipated energy as the main energy causing the propagation of crack and breakage of rock materials during the dynamic impact. In this case, the dissipated energy can be approximated as broken energy. The statistics of crushing energy under different working conditions are shown in **Figure 6**. **Figure 6** shows that the dissipated energy has an evident strain rate effect and temperature effect on the failure process of the granite specimen. Dissipated energy increases with an increase in the strain rate and becomes a quadratic parabola with an increase in temperature. The overall evolution law of the crushing energy of granite during the dynamic impact was consistent compared to the dynamic compressive strength

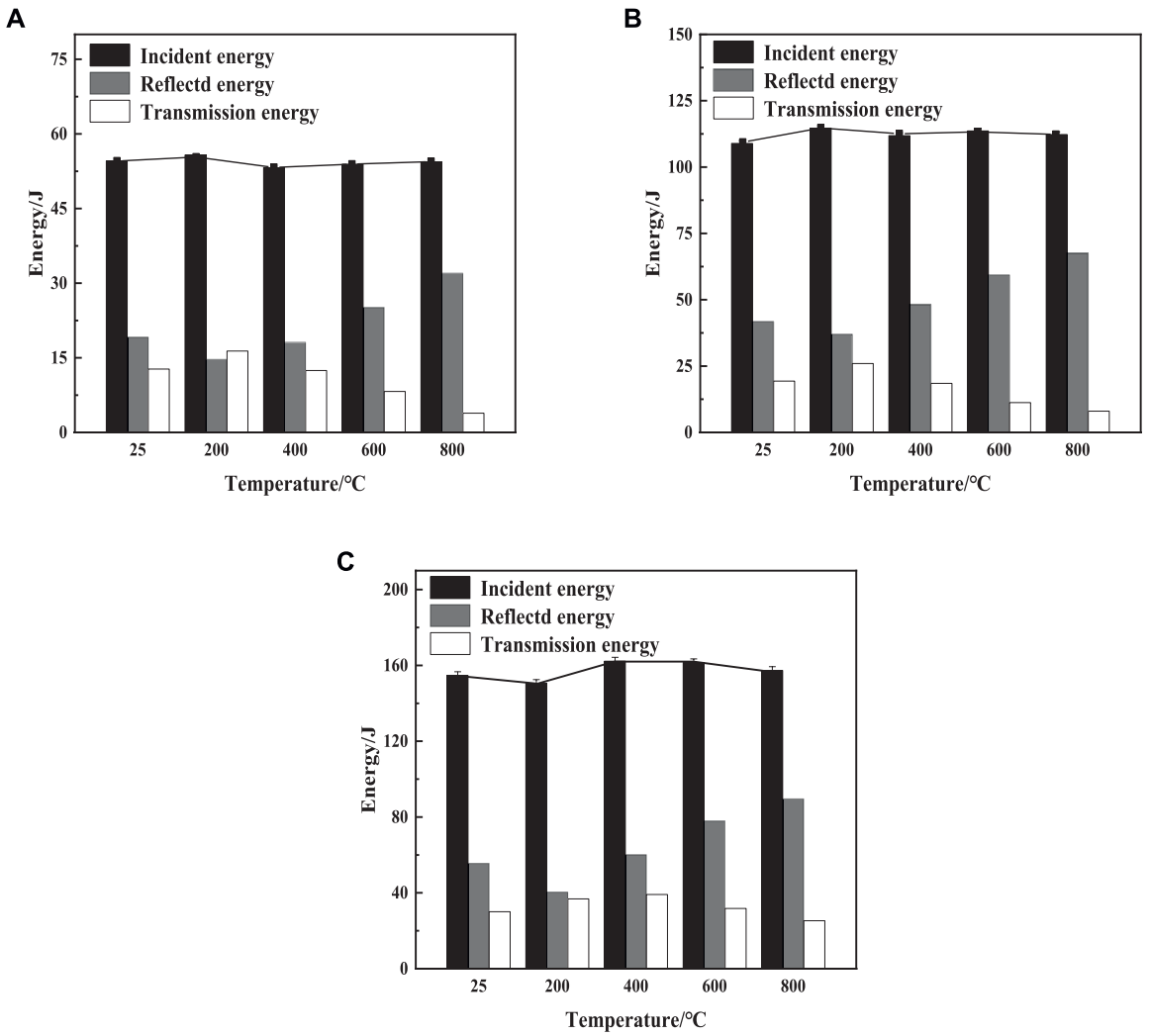

FIGURE 5 | Relationship curves of reflected and transmitted energies with incident energy at impact velocities of **(A)** 8.5 m/s, **(B)** 11.5 m/s, and **(C)** 13.5 m/s.

under different working conditions. This can also explain the strain rate and temperature effects on the dynamic compressive strength of granite from the perspective of energy dissipation.

Shape Features

The fracture morphology of the granite after high-temperature treatment is shown in **Figure 7**. The failure modes of the granite specimens exhibit obvious temperature and strain rate effects (**Figure 7**). With an increase in temperature and impact rate grades, both showed a trend of deepening crushing degree, increasing granular fragments, and gradually decreasing particles after crushing. Thus, it was concluded that the temperature and the impact rate influence the final failure mode of the granite specimen by affecting the energy dissipation during the impact. Under the same impact rate, the granite specimen gradually developed from splitting failure mode with a less fracture surface to compression failure mode, with an increase in temperature and strain rate grade.

The distribution of rock fragmentation reflects the overall effect on it under the combined influence of temperature and impact load (Xu and Liu, 2012). A standard circular hole screen was used to screen-crushed granite specimens. Statistical analysis was conducted to obtain the distribution of broken lumpiness in granite specimens at different impact rates and temperature levels. The method introduced by Xu and Liu (2012) was implemented to calculate the average fragmentation, dm, of the granite specimens using **the**following equation (**Figure 8**):

$$d_m = \sum (r_i d_i) \Big/ \sum r_i, \tag{4}$$

where d_i is the average size of residual screen fragments (0.15, 0.4, 0.75, 1.75, 3.75, 7.5, 12.5, 17.5, 22.5, and 37.5 mm) and r_i is the percentage of residual screen fragments in the total mass of fragments.

It can be seen from **Figure 8** that the average fragmentation of granite ranges from 7.22 to 34.27 mm. At the same impact velocity, and

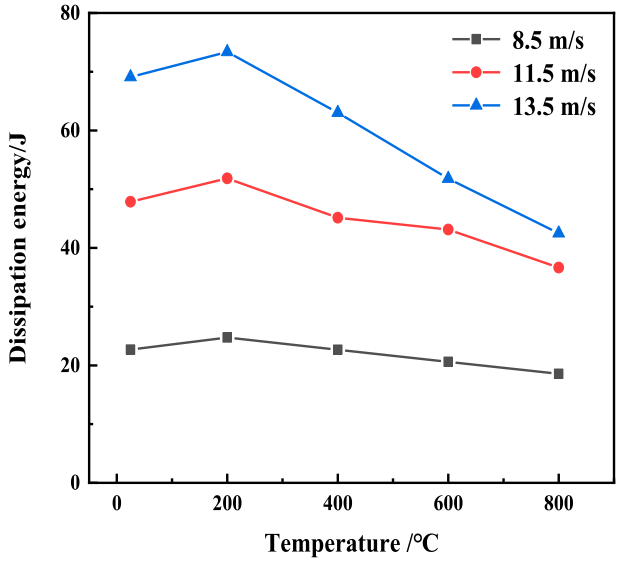

FIGURE 6 | Variations in dissipated energy under different working conditions.

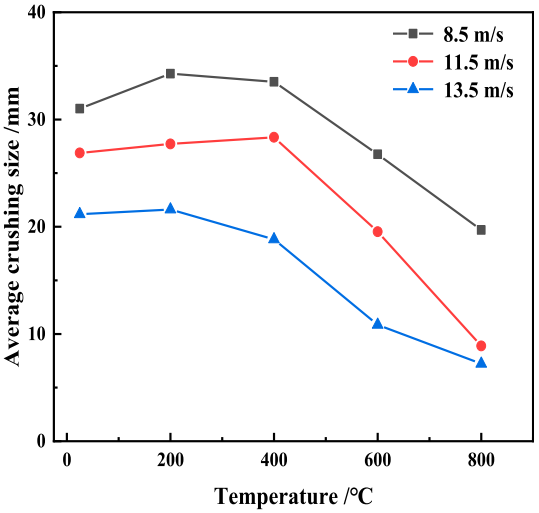

FIGURE 8 | Average fragment size distribution of granite.

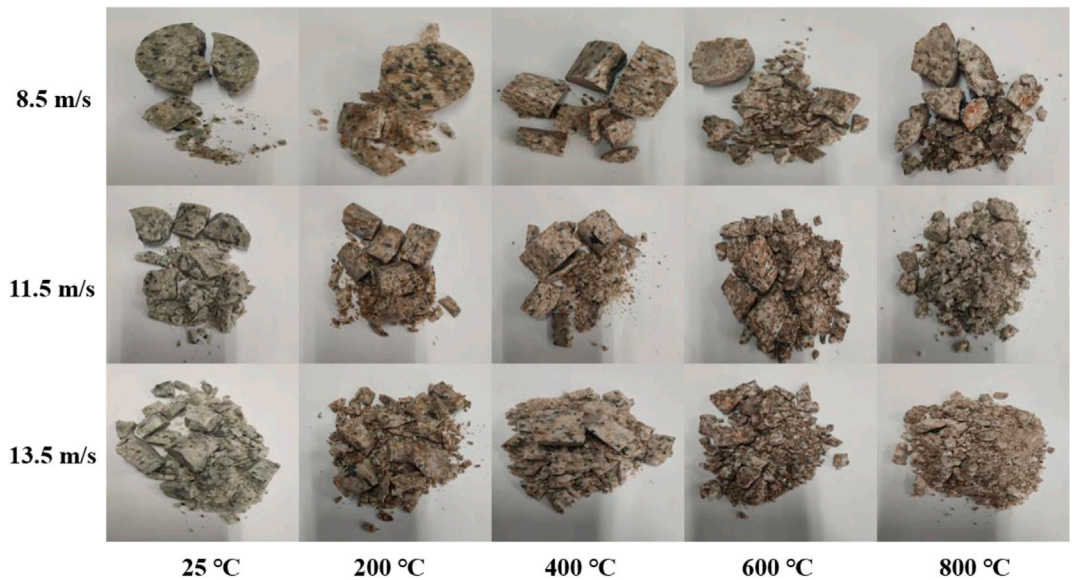

FIGURE 7 | Failure modes of granite under different temperatures and impact velocities.

an increasing temperature grade, the average fragmentation degree of granite increases gradually and reaches a maximum value between 200 and 400°C. When the heating temperature exceeded 400°C, the average fragmentation of granite began to decrease, reaching a minimum value at 800°C. This indicates that there exists a threshold temperature that affects the variation in the average fragmentation size of granite. In our experiments for the present study, the threshold temperature ranged between 200 and 400°C. Under the same heating temperature grade, the average fragmentation of granite showed a gradually increasing trend with an increase in the impact rate grade.

According to the fractal dimension, D_b of the mass–frequency relationship of the screening test, and the calculation formula can be expressed as follows (Xu and Liu, 2012):

$$lg\left(M_{x_0}/M_T\right) = \left(3 - D_b\right) lg\left(\frac{x_0}{x_m}\right), \tag{5}$$

where M_{x_0} and M_T are the cumulative mass of the material under the sieve and the total mass of fragments, respectively; x_0 and x_m represent the size of the broken fragments and maximum size of the fragments, respectively.

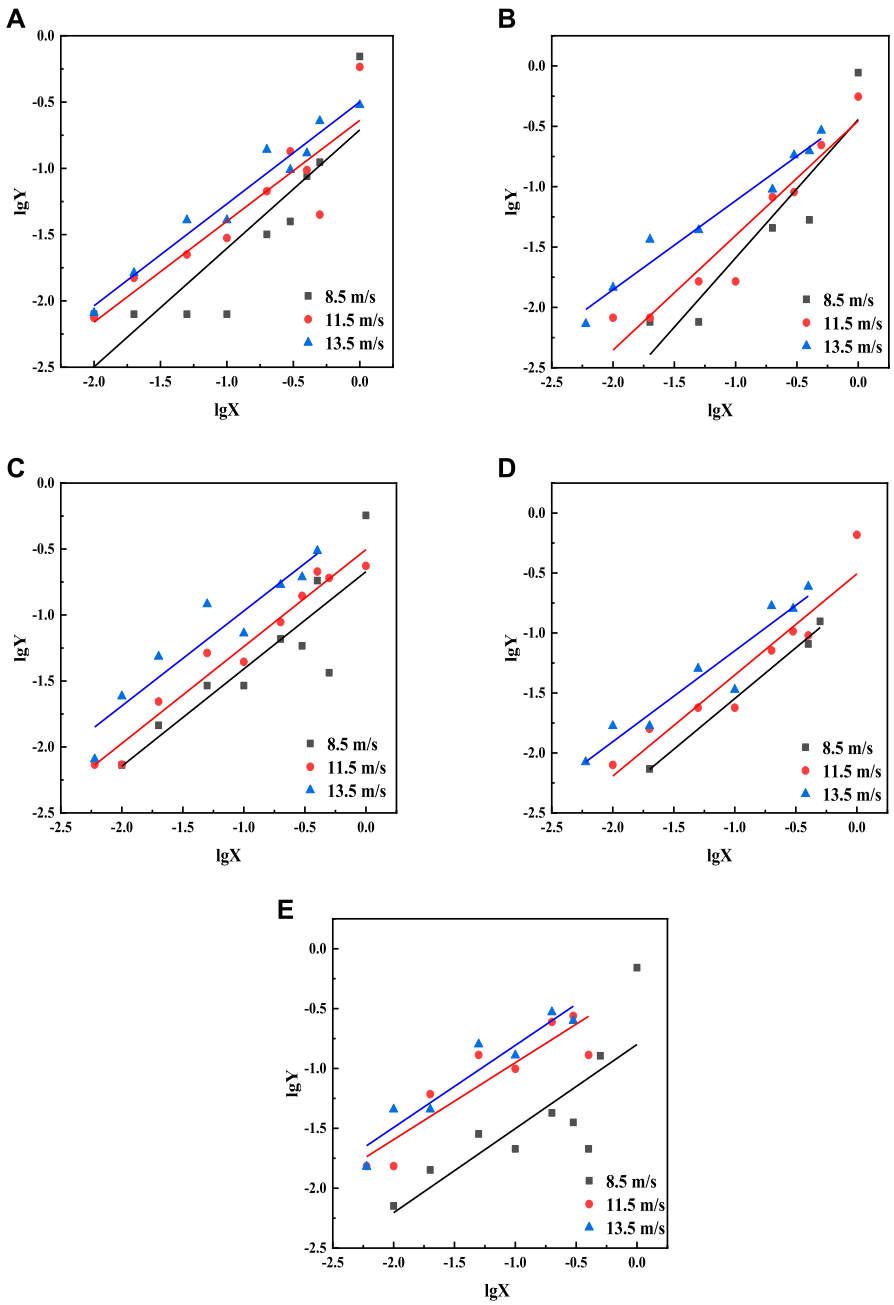

FIGURE 9 | lgY–lgX curves: **(A)** 25°C, **(B)** 200°C, **(C)** 400°C, **(D)** 600°C, and **(E)** 800°C.

The fractal dimension D_b of granite fragmentary lumpiness can be obtained by linearly fitting $M_{x_0}/M_T = Y$, $x_0/x_m = X$ on the data points in the lgY–lgX-type logarithmic coordinate system. The logarithmic coordinate curve for the calculation of the dynamic impact fractal dimension of granite after high-temperature treatment is shown in **Figure 9**. The statistical results for the fractal dimension are listed in **Table 2**.

It can be observed from **Table 2** that the fitting line has a good correlation. With an improvement in the impact rate grade, the correlation of the fitting increases continuously. In the dynamic compression test, the fractal dimension of the granite fluctuated between 2.0138 and 2.3640. The fractal dimension is not only related to the strain rate but also to the properties of the rock itself (Ji et al., 2020). Under the condition of a constant impact load, the change in fractal dimension with temperature is opposite to the peak stress change in the dynamic impact of granite. The smaller the peak stress of granite, the more severe the degree of breakage, and the larger the fractal dimension. The change in the fractal dimension indirectly reflects the influence of temperature and impact load coupling on the mechanical properties of granite (Xu and Liu, 2012).

TABLE 2 | Fractal dimensions and fitting degrees at different temperatures.

Temperature/°C	8.5 m/s		11.5 m/s		13.5 m/s	
	Fractal dimension	Fitting degree	Fractal dimension	Fitting degree	Fractal dimension	Fitting degree
25	2.1061	0.7715	2.1829	0.8246	2.2332	0.9604
200	2.0138	0.8575	2.0908	0.9143	2.1528	0.9672
400	2.1536	0.9897	2.2060	0.9038	2.2417	0.9203
600	2.2030	0.7680	2.2655	0.9572	2.2799	0.8793
800	2.2975	0.6542	2.3372	0.8449	2.3640	0.8825

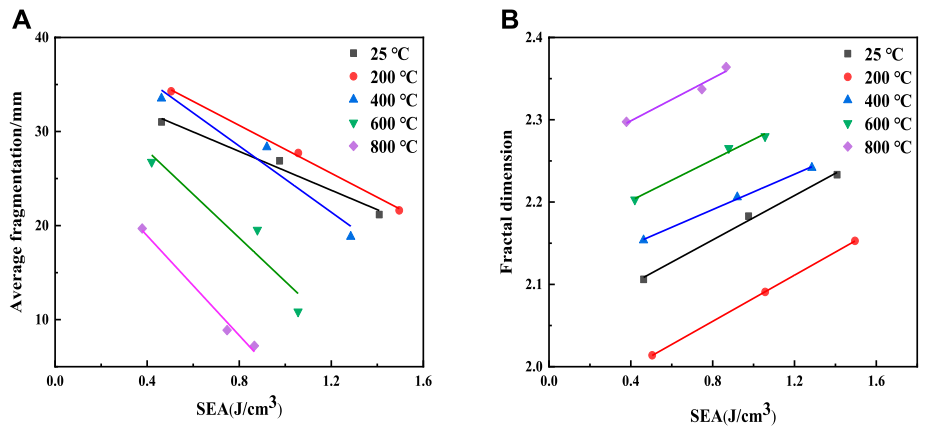

FIGURE 10 | Relationship of **(A)** average fragmentation and **(B)** fractal dimensions with energy consumption density.

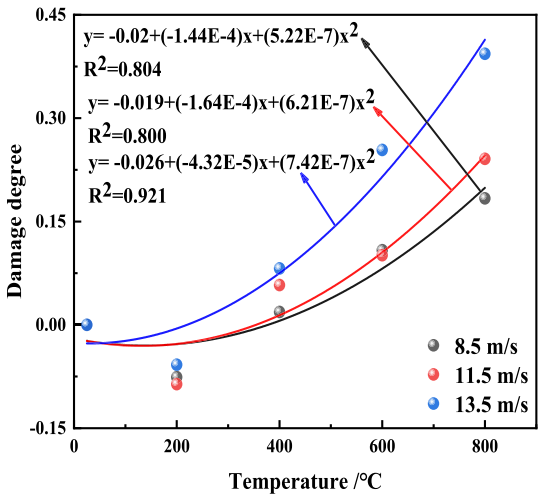

FIGURE 11 | Temperature damage degrees in different working conditions.

Relationship Between Fractal Characteristics and Energy Dissipation

To explore the quantitative relationship between the macro- and micro-characteristics of granite after high-temperature treatment, this study established the relationship between the fractal dimension theory and the associated characterization indexes in the energy dissipation theory. **Figure 10** shows the relationship among average fragmentation, fractal dimension, and energy consumption density.

As shown in **Figure 10**, under the same temperature grade, the average fragmentation of granite decreases linearly with an increase in the energy consumption density. The fractal dimension increased linearly with energy consumption density. The smaller the mean fragmentation, the larger is the fractal dimension. This indicates that the crushing degree of granite was higher during the dynamic impact process. Rock failure is the process of the development, expansion, and coalescence of microfractures in the rock, which is the result of internal damage due to macroscopic failure. The development and propagation of microfractures require energy absorption. As energy consumption density increased, so did the energy absorbed by granite per unit volume during dynamic impact compression and the energy used for rock damage and fracture; this led to the development and expansion of microcracks in the rock. Consequently, the degree of breakage became more intense, the number of new cracks and fracture surfaces, output of small particle size fragments, and the fractal dimension increased, while the average fragmentation size decreased.

Degree of Damage Analysis

The failure process of the rock under a given impact load and temperature is caused by the damage to breakage (Yu et al.,

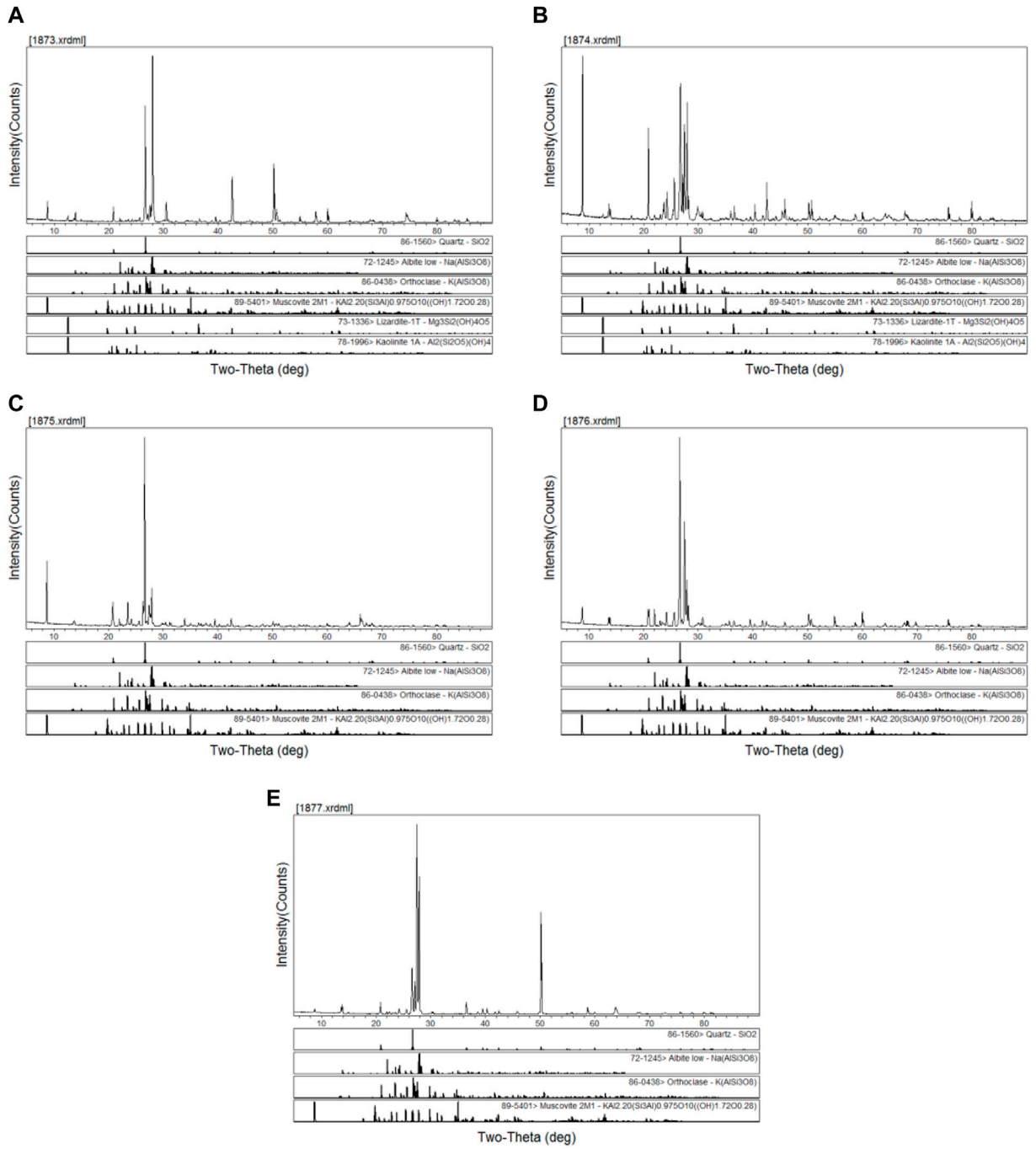

FIGURE 12 | X-ray diffraction phase analysis of granite at different temperatures: **(A)** 25°C, **(B)** 200°C, **(C)** 400°C, **(D)** 600°C, and **(E)** 800°C.

2020). The calculation of the degree of rock damage in this process forms the basis for constructing a dynamic constitutive equation of rock materials under different working conditions. So far, some studies have discussed the measurement and calculation methods for the rock damage degree from the perspective of non-destructive testing and damage testing. Non-destructive testing is mainly carried out through CT scanning of the damaged rock specimens (Wang et al., 2018), measurement of longitudinal wave velocity (Zuo et al., 2017), and other tests in a manner such that the test objects are not damaged. In contrast, the damage testing method mainly involves destructive mechanical experiments on the tested specimen; this method characterizes the damage degree of rock materials using data obtained from experiments

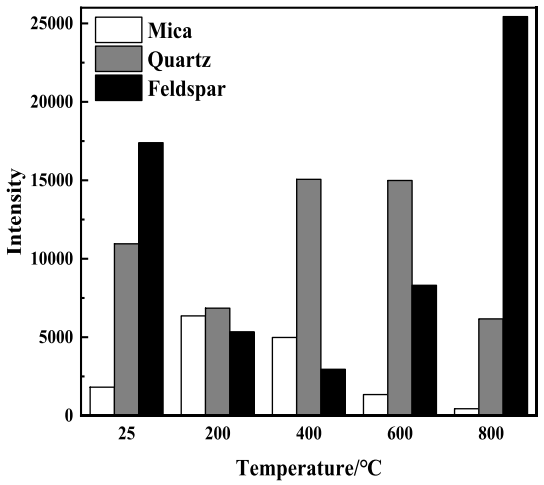

FIGURE 13 | Diffraction intensity of main mineral components of granite at different temperatures.

involving dynamic elastic modulus (Xu et al., 2020), dynamic compressive strength (Guo et al., 2017), energy dissipation (Zhao et al., 2019), breakage of the test specimen (Zhai, 2015), and development and expansion mode of cracks in the failure process (Li et al., 2020). Owing to the limitation of the experimental conditions, this study only considered the degree of damage from the perspective of the energy absorption value.

Based on the strain equivalence principle (He et al., 2018), **Eq. 6** was used to characterize the temperature damage from the perspective of energy dissipation:

$$D_{T(W)} = \frac{W_T - W_0}{1 - W_0}, \tag{6}$$

where $D_{T(W)}$ represents the damage factor, W_0 represents the dissipated energy at 25°C, and W_T represents the corresponding temperature dissipated energy.

It can be observed from **Figure 11** that $D_{T(W)}$ of different temperature grades presents a quadratic non-linear correlation under the same impact velocity. When the heating temperature ranges from 25 to 200°C, $D_{T(W)} < 0$. This reflects the strengthening effect of temperature on the dynamic mechanical properties of granite. When the heating temperature level exceeds 200°C, $D_{T(W)}$ shows an increasing trend with an increase in the heating temperature level. The results indicate that temperature degrades the dynamic mechanical properties of granite over time, which is consistent with the effect of temperature on the dynamic compressive strength. However, with the increase in impact velocity in the test, the energy used for crushing the rock increased, and the coupled effect of impact velocity and temperature aggravated the internal damage of the rock.

Analysis of Granite Facies Characteristics

X-ray diffraction (XRD) experiments were performed on granite at room temperature and high temperature to analyze the changes in the physical phase characteristics of granite before and after high-temperature treatment. The XRD patterns of granite at various temperatures are shown in **Figure 12**.

As shown in **Figure 12**, the mineral composition and primary components of granite tend to change at different temperature grades. The variation in the diffraction intensities of the main components is shown in **Figure 13**.

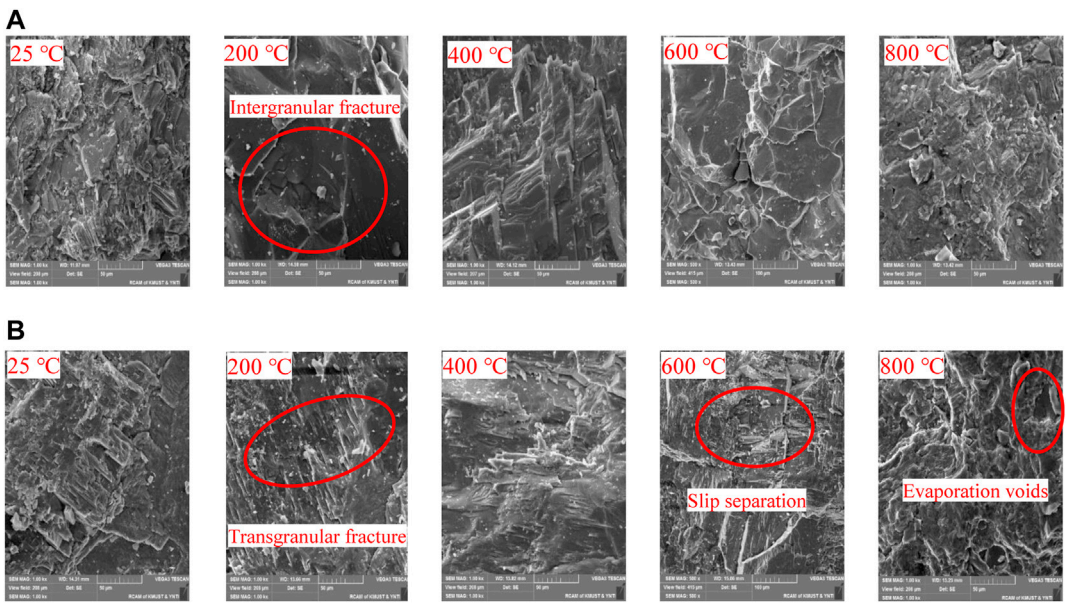

FIGURE 14 | Scanning electron microscopy image of granite at different conditions: **(A)** impact velocity of 11.5 m/s and **(B)** impact velocity of 13.5 m/s.

As shown in **Figure 13**, the primary mineral components of granite at normal temperatures are mica, quartz, feldspar, and small amounts of silicate minerals. When the heating temperature was 200°C, the diffraction intensity of mica increased to 6,354 counts, which continued to decrease with an increase in the heating temperature. When the heating temperature was 800°C, the diffraction intensity was 432 counts. With an increase in the heating temperature, the diffraction intensity of feldspar first decreased and then increased. When the heating temperature was 400°C, the diffraction intensity reached a minimum of 2,958 counts. Overall, the diffraction intensity of quartz was correlated with the change in mineral compositions, and the minimum diffraction intensity was observed at 800°C.

When the heating temperature was 200°C, the main mineral components in granite at normal temperature were the same. However, the effect of temperature on the diffraction intensity varied significantly; that is, the diffraction intensity of mica was greater than that of the other main mineral components, which exhibited similar diffraction intensities. Meanwhile, the grain was not structurally damaged, and the rock compressive strength improved significantly. When the temperature rose to 400°C, the diffraction intensity of quartz increased due to the effect of high temperature on the main mineral composition and decomposition reaction of silicate minerals. Between 400 and 600°C, α-quartz becomes β-modification. Subsequently, the crystal expanded and led to the formation of small cracks inside the rock, thereby weakening the cementation force between grains and decreasing the compressive strength of granite; this result is consistent with the apparent morphology of the granite specimen after the high-temperature treatment (**Figure 1**). When the temperature reaches 800°C, feldspar changes from a crystalline state to an amorphous state (Jia et al., 2021). Thus, after the high-temperature treatment, the granite strength decreases, failure strain increases, and the diffraction intensity fluctuates significantly compared to that in the normal temperature state. A change in the crystal structures of feldspar and quartz deteriorated the mechanical properties of the granite specimens. Meanwhile, decreasing the diffraction intensity of mica promotes the brittle–plastic transformation of granite specimens to a certain extent, which is consistent with the results of macroscopic mechanical experiments.

Analysis of Fracture Morphology After Dynamic Impact

A tungsten wire scanning electron microscope (SEM) was used to observe the fracture morphology of granite specimens after impact compression failure at 25–800°C, and study the influence of the impact rate and temperature on the fracture failure form of granite. The fracture morphologies are shown in **Figure 14**.

Figure 14 shows that under dynamic impact compression conditions, the fracture morphology of granite presents different failure forms under different working conditions (temperature grade and impact rate). At a constant temperature, intergranular fractures tend to be dominant when the impact rate is 11.5 m/s. With an increase in the impact rate, transgranular fractures increase to 200°C, as shown in **Figure 14**. When the temperature is 400°C, fine cracks appear on the rock. When the temperature rises to 600–800°C, plastic failure characteristics are observed (Liang et al., 2015; Tao et al., 2019).

A low shock rate, low incident energy, and the formation of a crack that extends along the crystal boundary lead to an intergranular fracture. Meanwhile, the impact velocity increases, leading to a rise in the incident energy and dynamic impact load time; in a short period of time, the internal atomic bonds in the crystal with low energy consumption cannot be damaged to produce a transgranular fracture. Although the internal mineral composition and granite microstructure are significantly correlated at high temperatures (such as between 25 and 400°C), the fracture morphology of the rock gives priority to brittle fracture, does not exhibit ductile fracture characteristics, and demonstrates a neat rock fracture morphology; meanwhile, the irregular fracture of quartz and feldspar led to a line shaped transgranular (conchoidal) fracture morphology, with a step cleavage plane fracture. During 600–800°C, the fracture morphology changed from a strip structure to a coarse block structure. The high temperature changed the rock's internal structure, the sliding and separation phenomenon indicates the brittle-to-plastic transformation of granite, which was consistent with the macro mechanical characteristics.

CONCLUSION

In this study, the granite subjected to high-temperature treatment was taken as the research object. The fragmentation morphology and the energy dissipation of the rock after normal (25°C) and high-temperature treatments (200°C, 400°C, 600°C, and 800°C) were studied using the SHPB device, while the fragmentation characteristics and dynamic mechanical properties of granite were elucidated. The crushing characteristics and the energy dissipation law of granite specimens affected by high temperatures in the SHPB experiment were also studied, while the temperature damage under different impact velocities was discussed with regard to energy dissipation. The main conclusions of this study are as follows:

1) Temperature and the strain rate affect the dynamic mechanical properties of granite and the energy dissipation during the failure process, which are closely related to the threshold value of the heating temperature grade. In the experiments conducted in this study, the threshold temperature is 200°C. Below 200°C, the transmitted energy first increases, and then decreases with an increase in the temperature grade; meanwhile, the transmitted energy exhibits an opposite change trend.

2) With an increase in the temperature grade, the failure mode of the rock changes from splitting failure to compression failure; the impact rate of ascension, which increases the energy density, tends to decrease the broken blocks of granite. Meanwhile, the fractal dimension increases with a rise in the energy consumption and density. Moreover, strain rate effects, broken blocks, changes in the fractal dimension, and the influence of temperature on rock mechanical characteristics are closely related; thus, these characteristics can reflect both the rock crushing processes to some extent.
3) From the perspective of energydissipation characterization of the rock damage degree, a quadratic non-linear relationship is observed with temperature. When the heating temperature range is 25–200°C, $D_{T(W)} < 0$; this reflects the effect of temperature on the rock's mechanical properties of the reinforcement. Meanwhile, the damage degree increased with a rise in the temperature, which is consistent with the influence law of temperature on the dynamic compressive strength.
4) High temperatures affect the compositional characteristics of granite and change its mechanical properties. A decrease in the muscovite content and the transformation of quartz and feldspar crystals led to the gradual deterioration of the mechanical behavior of granite. At a same temperature level, it is observed that the higher the impact velocity, the higher is the proportion of transgranular fractures. With an increase in the heating temperature, the fracture morphology becomes more complex and ductile fracture failure characteristics are observed, thus indicating that the rock underwent a brittle-to-plastic transformation under the influence of high temperature.

DATA AVAILABILITY STATEMENT

The original contributions presented in the study are included in the article/Supplementary Material, further inquiries can be directed to the corresponding author.

AUTHOR CONTRIBUTIONS

Conceptualization: HA and LL; methodology: HA and LL; formal analysis: HA and LL; investigation: YW; writing—original draft preparation: HA and YW; and funding acquisition: LL. All authors read and agreed to the published version of the manuscript.

FUNDING

This research was funded by the National Natural Science Foundation of China (grant Nos.11862010 and 51964023).

REFERENCES

Bandini, A., and Berry, P. (2012). Influence of Marble's Texture on its Mechanical Behavior. *Rock Mech. Rock Eng.* 46 (4), 785–799. doi:10.1007/s00603-012-0315-1

Brotóns, V., Tomás, R., Ivorra, S., and Alarcón, J. C. (2013). Temperature Influence on the Physical and Mechanical Properties of a Porous Rock: San Julian's Calcarenite. *Eng. Geol.* 167, 117–127. doi:10.1016/j.enggeo.2013.10.012

Ge, Z., and Sun, Q. (2018). Acoustic Emission (AE) Characteristics of Granite after Heating and Cooling Cycles. *Eng. Fracture Mech.* 200, 418–429. doi:10.1016/j.engfracmech.2018.08.011

Guo, H., Guo, W., Zhai, Y., and Su, Y. (2017). Experimental and Modeling Investigation on the Dynamic Response of Granite after High-Temperature Treatment under Different Pressures. *Const. Build. Mater.* 155, 427–440. doi:10.1016/j.conbuildmat.2017.08.090

He, A. L., Wang, Z. L., and Bi, C. C. (2018). Study on Thermal Damage Characteristics and Mechanism of Huashan Granite. *Hydro-Science and Engineering* 01, 95–101. doi:10.16198/j.cnki.1009-640X.2018.01.014

He, J. F. (1994). Resource Distribution and Geological Genesis of marble and Granite in Some Places, Prefectures and Counties in Yunnan Province. *Yunnan Building Mater.* 000 (03), 4–7.

Hong, L., Zhou, Z.-l., Yin, T.-b., Liao, G.-y., and Ye, Z.-y. (2009). Energy Consumption in Rock Fragmentation at Intermediate Strain Rate. *J. Cent. South. Univ. Technol.* 16 (4), 677–682. doi:10.1007/s11771-009-0112-5

Hu, S. S., Wang, L. L., Song, L., and Zhang, L. (2015). Review of the Development of Hopkinson Pressure Bar Technology in China. *Explos. Shock Waves* 34 (06), 641–657. doi:10.11883/1001-1455(2014)06-0641-17

Imani, M., Nejati, H. R., and Goshtasbi, K. (2017). Dynamic Response and Failure Mechanism of Brazilian Disk Specimens at High Strain Rate. *Soil Dyn. Earthquake Eng.* 100, 261–269. doi:10.1016/j.soildyn.2017.06.007

Ji, J. J., Li, H. T., Wu, F. M., and Yao, Q. (2020). Fractal Characteristics of Rock Fracture under Impact Loading. *Shock Vib.* 39 (13), 176–183. doi:10.13465/j.cnki.jvs.2020.13.026

Jia, P., Yang, Q. J., Liu, D. Q., Wang, S. H., and Zhao, Y. (2021). Physical and Mechanical Properties and Micro-fracture Characteristics of High Temperature Granite after Water Cooling. *Rock Soil Mech.* 42 (06), 1568–1578. doi:10.16285/j.rsm.2020.1383

Li, D. Y., Hu, C. W., and Zhu, Q. Q. (2020). Experimental Study on Mechanical Properties and Failure Law of Precast Fractured Granite under Dynamic and Static Combined Loading. *Chin. J. Rock Mech. Eng.* 39 (06), 1081–1093. doi:10.13722/j.cnki.jrme.2019.1089

Li, G., Sun, Y., and Qi, C. (2021). Machine Learning-Based Constitutive Models for Cement-Grouted Coal Specimens under Shearing. *Int. J. Mining Sci. Techn.* 31, 813–823. doi:10.1016/j.ijmst.2021.08.005

Liang, C. Y., Wu, S. R., and Li, X. (2015). Study on fine-microscopic Characteristics of Granite Fracture under Uniaxial Compression in the Range of Medium and Low Strain Rates. *Chin. J. Rock Mech. Eng.* 34 (S1), 2977–2986. doi:10.13722/j.cnki.jrme.2014.0701

Liu, S., and Xu, J. Y. (2014). Study on the Effect of High Temperature on the Dynamic Compression Mechanical Properties of Granite. *Vibration Shock* 33 (04), 195–198. doi:10.13465/j.cnki.jvs.2014.04.034

Liu, S., and Xu, J. (2015). An Experimental Study on the Physico-Mechanical Properties of Two post-high-temperature Rocks. *Eng. Geol.* 185, 63–70. doi:10.1016/j.enggeo.2014.11.013

Malik, A., Chakraborty, T., and Rao, K. S. (2018). Strain Rate Effect on the Mechanical Behavior of basalt: Observations from Static and Dynamic Tests. *Thin-Walled Struct.* 126, 127–137. doi:10.1016/j.tws.2017.10.014

Mishra, S., Chakraborty, T., Matsagar, V., Loukus, J., and Bekkala, B. (2018). High Strain-Rate Characterization of Deccan Trap Rocks Using SHPB Device. *J. Mater. Civ. Eng.* 30 (5), 04018059. doi:10.1061/(asce)mt.1943-5533.0002229

Qi, C. C., Yang, X. Y., Li, G. C., Chen, Q. S., and Sun, Y. T. (2021). Summary and prospect of the Application of New Generation Artificial Intelligence in Mine Filling. *J. Coal* 46 (02), 688–700. doi:10.13225/j.cnki.jccs.xr20.1704

Sasmito, A. P., Kurnia, J. C., Birgersson, E., and Mujumdar, A. S. (2015). Computational Evaluation of thermal Management Strategies in an Underground Mine. *Appl. Therm. Eng.* 90, 1144–1150. doi:10.1016/j.applthermaleng.2015.01.062

Shu, R.-h., Yin, T.-b., Li, X.-b., Yin, Z.-q., and Tang, L.-z. (2019). Effect of thermal Treatment on Energy Dissipation of Granite under Cyclic Impact Loading. *Trans. Nonferrous Met. Soc. China* 29 (2), 385–396. doi:10.1016/s1003-6326(19)64948-4

Tao, M., Wang, J., Li, Z. W., Hong, Z. X., Wang, Y. Q., and Zhao, R. (2019). Fine-microscopic Experimental Study on Fracture Surface of Granite Layer under Impact Loading. *J. Rock Mech. Eng.* 38 (11), 2172–2181. doi:10.13722/j.cnki.jrme.2019.0185

Wang, X.-Q., Schubnel, A., Fortin, J., Guéguen, Y., and Ge, H.-K. (2013). Physical Properties and Brittle Strength of Thermally Cracked Granite under Confinement. *J. Geophys. Res. Solid Earth* 118 (12), 6099–6112. doi:10.1002/2013jb010340

Wang, Y., Hou, Z. Q., and Hu, Y. Z. (2018). *In Situ* X-ray Micro-CT for Investigation of Damage Evolution in Black Shale under Uniaxial Compression. *Environ. Earth Sci.* 77 (20), 1–12. doi:10.1007/s12665-018-7904-6

Wang, L. l. (2005). *Stress Wave Foundation [M]*. Beijing: National Defense Industry Press, 52–60.

Wu, R. J., Li, H. B., Li, X. F., Yue, H. Z., Yu, C., and Xia, X. (2019). Study on Compressive Mechanical Properties of Layered Phyllite under Different Impact Loads. *J. Rock Mech. Eng.* (S2), 3304–3312. doi:10.13722/j.cnki.jrme.2018.1084

Wu, R. J., Li, H. B., Li, X. F., Yu, C., Xia, X., and Liu, L. W. (2020). Energy Consumption and Fragmentation Characteristics of Layered Rock under Impact Loading. *J. Coal* 45 (03), 1053–1060. doi:10.13225/j.cnki.jccs.2019.0266

Xia, C. J., Xie, H. P., Ju, Y., and Zhou, H. W. (2006). Experimental Study on Energy Dissipation of Porous Rock under Impact Loading. *Eng. Mech.* 23 (09), 1–5. doi:10.3969/j.issn.1000-4750.2006.09.001

Xie, H. P. (2019). Research Progress of Deep Rock Mass Mechanics and Mining Theory. *J. Coal* 44 (05), 1283–1305. doi:10.13225/j.cnki.jccs.2019.6038

Xu, J. Y., and Liu, S. (2012). Analysis of Fractal Characteristics of marble Fragments in Impact Loading Test. *Rock Soil Mech.* 33 (11), 3225–3229. doi:10.16285/j.rsm.2012.11.005

Xu, J. Y., and Shi, L. (2013). Analysis of Energy Consumption Law of Rock Deformation and Failure Process under High Temperature in SHPB Test. *J. Rock Mech. Eng.* 32 (S2), 3109–3115.

Xu, J., Kang, Y., Wang, Z., Wang, X., Zeng, D., and Su, D. (2020). Dynamic Mechanical Behavior of Granite under the Effects of Strain Rate and Temperature. *Int. J. Geomech.* 20 (2), 04019177. doi:10.1061/(asce)gm.1943-5622.0001583

Yin, T. B., Li, X. B., Wang, B., Yin, Z. Q., and Jin, J. F. (2011). Study on Mechanical Properties of sandstone under Dynamic Compression after High Temperature. *J. Geotechn. Eng.* 33 (05), 777–784.

Yin, T.-b., Peng, K., Wang, L., Wang, P., Yin, X.-y., and Zhang, Y.-l. (2016a). Study on Impact Damage and Energy Dissipation of Coal Rock Exposed to High Temperatures. *Shock Vib.* 2016, 1–10. doi:10.1155/2016/5121932

Yin, T.-b., Shu, R.-h., Li, X.-b., Wang, P., and Liu, X.-l. (2016b). Comparison of Mechanical Properties in High Temperature and thermal Treatment Granite. *Trans. Nonferrous Met. Soc. China* 26 (7), 1926–1937. doi:10.1016/s1003-6326(16)64311-x

Yin, Z., Chen, W., Hao, H., Chang, J., Zhao, G., Chen, Z., et al. (2019). Dynamic Compressive Test of Gas-Containing Coal Using a Modified Split Hopkinson Pressure Bar System. *Rock Mech. Rock Eng.* 53, 815–829. doi:10.1007/s00603-019-01955-w

Yu, L., Peng, H. W., Li, G. W., Zhang, Y., Han, Z. H., and Zhu, H. Z. (2020). Experimental Study on Granite under High Temperature-Water Cooling Cycle. *Rock Soil Mech.* 42 (04), 1025–1035. doi:10.16285/j.rsm.2020.1154

Yuan, L., Xue, J. H., Liu, Q. S., and Liu, B. (2011). Surrounding Rock Control Theory and Support Technology of Deep Rock Roadway in Coal Mine. *J. China Coal Soc.* 36 (04), 535–543. doi:10.13225/j.cnki.jccs.2011.04.014

Zhai, Y. (2015). Space Wave Equation Considering Damage-Induced Weakening and Strain Rate Dependency of Rock. *Teh. Vjesn.* 22 (4), 1035–1042. doi:10.17559/tv-20150406112756

Zhang, R. R., and Jing, L. W. (2018). Analysis of the Relationship between Crushing Degree and Energy Dissipation of Deep sandstone after the Action of High and Low Temperature in SHPB Test. *J. Coal* 43 (07), 1884–1892. doi:10.13225/j.cnki.jccs.2017.1493

Zhao, Z., Ma, W., Fu, X., and Yuan, J. (2019). Energy Theory and Application of Rocks. *Arab J. Geosci.* 12 (15), 1–26. doi:10.1007/s12517-019-4617-4

Zhou, Y. X., Xia, K., Li, X. B., Li, H. B., Ma, G. W., Zhao, J., et al. (2012). Suggested Methods for Determining the Dynamic Strength Parameters and Mode-I Fracture Toughness of Rock Materials. *Int. J. Rock Mech. Min.* 49, 105–112. doi:10.1007/978-3-319-07713-0_3

Zuo, J.-P., Wang, J.-T., Sun, Y.-J., Chen, Y., Jiang, G.-H., and Li, Y.-H. (2017). Effects of thermal Treatment on Fracture Characteristics of Granite from Beishan, a Possible High-Level Radioactive Waste Disposal Site in China. *Eng. Fracture Mech.* 182, 425–437. doi:10.1016/j.engfracmech.2017.04.043

Conflict of Interest: The authors declare that the research was conducted in the absence of any commercial or financial relationships that could be construed as a potential conflict of interest.

Publisher's Note: All claims expressed in this article are solely those of the authors and do not necessarily represent those of their affiliated organizations, or those of the publisher, the editors, and the reviewers. Any product that may be evaluated in this article, or claim that may be made by its manufacturer, is not guaranteed or endorsed by the publisher.